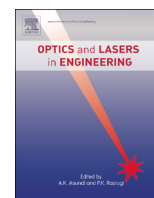




ELSEVIER

Contents lists available at ScienceDirect

Optics and Lasers in Engineering

journal homepage: www.elsevier.com/locate/optlaseng

Programmable aperture microscopy: A computational method for multi-modal phase contrast and light field imaging

Chao Zuo^{a,b,*}, Jiasong Sun^{a,b}, Shijie Feng^{a,b}, Minliang Zhang^{a,b}, Qian Chen^b

^a Smart Computational Imaging Laboratory (SCILab), Nanjing University of Science and Technology, Nanjing, Jiangsu Province 210094, China

^b Jiangsu Key Laboratory of Spectral Imaging & Intelligent Sense, Nanjing University of Science and Technology, Nanjing, Jiangsu Province 210094, China

ARTICLE INFO

Article history:

Received 17 July 2015

Received in revised form

1 December 2015

Accepted 17 December 2015

Keywords:

Microscopy

Phase retrieval

Multi-modal imaging

Quantitative phase microscopy

Light field microscopy

ABSTRACT

We demonstrate a simple and cost-effective programmable aperture microscope to realize multi-modal computational imaging by integrating a programmable liquid crystal display (LCD) into a conventional wide-field microscope. The LCD selectively modulates the light distribution at the rear aperture of the microscope objective, allowing numerous imaging modalities, such as bright field, dark field, differential phase contrast, quantitative phase imaging, multi-perspective imaging, and full resolution light field imaging to be achieved and switched rapidly in the same setup, without requiring specialized hardware and any moving parts. We experimentally demonstrate the success of our method by imaging unstained cheek cells, profiling microlens array, and changing perspective views of thick biological specimens. The post-exposure refocusing of a butterfly mouthpart and RFP-labeled dicot stem cross-section is also presented to demonstrate the full resolution light field imaging capability of our system for both translucent and fluorescent specimens.

© 2015 Elsevier Ltd. All rights reserved.

1. Introduction

Computational microscopy is an emerging technology which extends the capabilities of optical microscopy with the combination of optical coding and computational decoding. It provides us with novel imaging functionalities or improved imaging performance which are difficult or impossible to achieve using a conventional microscopic system. For example, quantitative phase microscopy enables biological samples to be visualized and quantified without the need for specific staining or labelling by incorporating interferometry or phase retrieval algorithms with conventional microscopy [1–4]. Structured illumination microscopy and Fourier ptychographic microscopy utilize angularly varying oblique illuminations and synthetic aperture algorithms to bypass the resolution limit defined by the microscopic objective [5–7]. Light field microscopy captures 4D light fields that allow digital refocusing or changing perspective of images via post-processing [8,9].

Recent advance in LED lighting and digital display technology provide new opportunities for active digital illumination and imaging control for advancing microscopy. By integrating a spatial light modulator (SLM) or a video projector into the illumination or

imaging path of the microscope, one gains the flexibility to produce sophisticated illumination patterns or dynamically switchable illumination sources with no moving components [10,11]. However, since the SLM is a technically complex device, these systems end up being heavy, bulky, and expensive. Alternatively, the active illumination control can be realized by replacing the condenser with a matrix of LEDs [12–14]. The LED-based condenser-free scheme provides a simple and cost-effective solution to realizing multi-modal contrast enhancement imaging but with a significantly reduced light collecting efficiency. Recently, instead of using a LED matrix, the use of a low cost liquid crystal display (LCD) to achieve programmable condenser illumination control has been reported [15,16]. In those methods, the condenser lens of a conventional microscope is kept unchanged but the condenser diaphragm was replaced a programmable LCD. The LCD-based programmable condenser techniques increase the photon budget and provide more flexibilities for controlling spatial coherence and microscope illumination over the LED-based condenser-free approaches.

In this paper, we present the programmable aperture microscope (PAM) to achieve multi-modal computational imaging. By integrating a programmable LCD as a low-cost transmissive spatial light modulator into the imaging aperture plane of the microscope, different spatial frequencies or angular components of the optical field can be directly manipulated. By properly choosing different binary patterns displayed on the LCD, the traditional methods of classic microscopy, including bright field, dark field,

* Corresponding author.

E-mail addresses: surpasszuo@163.com (C. Zuo), chenqian@njjust.edu.cn (Q. Chen).

differential phase contrast imaging can be realized without requiring specialized hardware components and any moving parts. Furthermore, it allows the quantitative phase of the sample to be measured non-interferometrically even with the use of an extended incoherent source from a standard microscope condenser. Finally, it achieves light field imaging at full sensor resolution through multiple exposures, without spatio-angular resolution trade-offs which are often inevitable in conventional microlens array based light field imaging. To the best of our knowledge, this is the first report of using a low cost LCD in the Fourier plane of the imaging path for multi-modal computational imaging and full sensor resolution light field microscopy. Compared with previously reported computational microscopic schemes based on programmable illuminations by using a LED array [12–14] or a programmable LCD [15,16], the reported PAM has the following advantages: first, the 4D dataset captured by angularly varying illuminations is a good approximation of the light field only in certain extremely simplified conditions (the sample should be angle-shift invariant respect to the incident light field, which in turn requires that the sample to be weak scattering or sufficiently thin) [17], while our approach gives one direct access to the precise 4D light field, which is independent of sample characteristics. Second, not just limited to conventional amplitude or phase specimens, our light field imaging approach can also be applied to fluorescent or self-luminous specimens. Finally, the programmable aperture module can be designed as a passive add-on that can be incorporated into most standard bright field or fluorescence microscopes with no hardware modifications.

2. System setup

The layout of the PAM is shown in Fig. 1. The whole system is built based on a commercial inverted infinity-corrected microscope (Olympus IX83), which itself is composed of a collector lens, condenser associated with aperture diaphragm, objective, reflective mirror (M_1), and tube lens, producing a magnified image of the specimen at the camera output port (image plane). The light from the built-in halogen lamp passes through a green interference filter (central wavelength $\lambda = 550$ nm, 45 nm bandwidth) to create quasi-monochromatic illuminations. To gain access to the rear aperture of the microscope objective, an additional 4f relay system is introduced, with the LCD located at the central Fourier

plane. In this case, the rear focal plane of the objective is imaged onto the LCD surface, and then modulated by the binary displayed pattern (to pass or to be blocked). The LCD is an Electronic Assembly DOGXL160-7 display with a resolution of 160×104 and 20 Hz frame rate. The panel size of the LCD is 78×61 mm (3.3 in.), which is sufficient to cover the entire spectral spread at the rear aperture of the microscope objective. The LCD is controlled by computer software via USB with an Atmel ATmega88 microcontroller. An AVI format movie clip (Media 1) is included to demonstrate different patterns shown on the display under our software control.

3. Results

3.1. Multi-modal contrast-enhancement imaging

We first demonstrate the flexibility of our PAM to realize contrast-enhancement imaging of unstained transparent samples. Fig. 2 clearly illustrates the various imaging modalities images of unstained cheek cells and the corresponding binary patterns displayed on the LCD. The sample is imaged by standard Olympus objective with magnification $10 \times$ (UPLFLN10X, $NA_{obj} = 0.3$) in the Köhler illumination configuration with illumination numerical aperture $NA_{ill} = 0.1$. For bright field imaging, we just display a clear background so that all light arriving the rear focal plane can pass through the LCD. As shown in Fig. 2(a), the sample is difficult to visualize under conventional bright field microscopy because the absorption and scattering are too weak to produce any contrast. However, once we block out the central part of light within the circle, allowing only scattered light goes on, a dark field image can be obtained. The increase in contrast is evident in Fig. 2(b), where the edges or boundaries of the cells are clearly highlighted in white against a dark background. It should be noted that in conventional dark field imaging, the illumination NA overfills the objective NA by using specialized condenser or diaphragm. While our approach can achieve similar effect by active controlling the light at the detection path without additional optics, albeit with a reduced illumination aperture.

3.2. Differential phase contrast and quantitative phase imaging

Our PAM can also be used for phase contrast imaging and quantitative phase imaging. By far, the most popular phase contrast imaging techniques employed in commercial microscopes are Zernike phase contrast and differential-interference contrast (DIC). However, both of them require specialized optics and provide images where phase and amplitude information is mixed. As an alternative to DIC, differential phase contrast (DPC) can produce a phase contrast image that looks similar to DIC, but with better linearity with respect to the phase gradient. DPC was originally proposed in the field of scanning electron or optical microscopy based on a split-detector [18], and recently has been adapted to wide-field optical microscopy based on asymmetric illumination [19,13]. By taking two images with two opposite but complementary illumination directions, the DPC image can be computed as their normalized difference. In this work, instead of changing the illumination directions, we can arrive another wide-field equivalent of the DPC based on split-aperture. By displaying two complementary (left-half and right half) patterns as shown in Fig. 2(c), the DPC image can be recovered by

$$D_x = \frac{I_R - I_L}{I_R + I_L} \quad (1)$$

The similar process may be repeated for realizing top-bottom DPC, with top half and bottom half patterns sequentially displayed, as

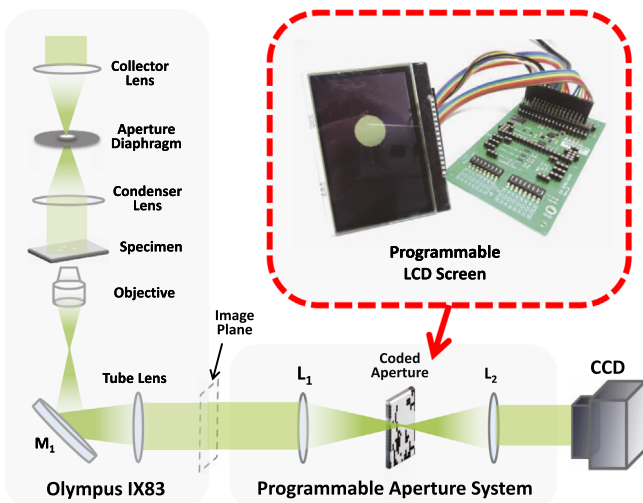


Fig. 1. Schematic setup for the PAM system. M_1 , mirrors; L_1 , L_2 , lenses (focal length $f_1 = 250$ mm, focal length $f_2 = 150$ mm). The boxed inset shows a photograph of the LCD, which allows dynamic attenuation mask patterns to be encoded under software control (Media 1).

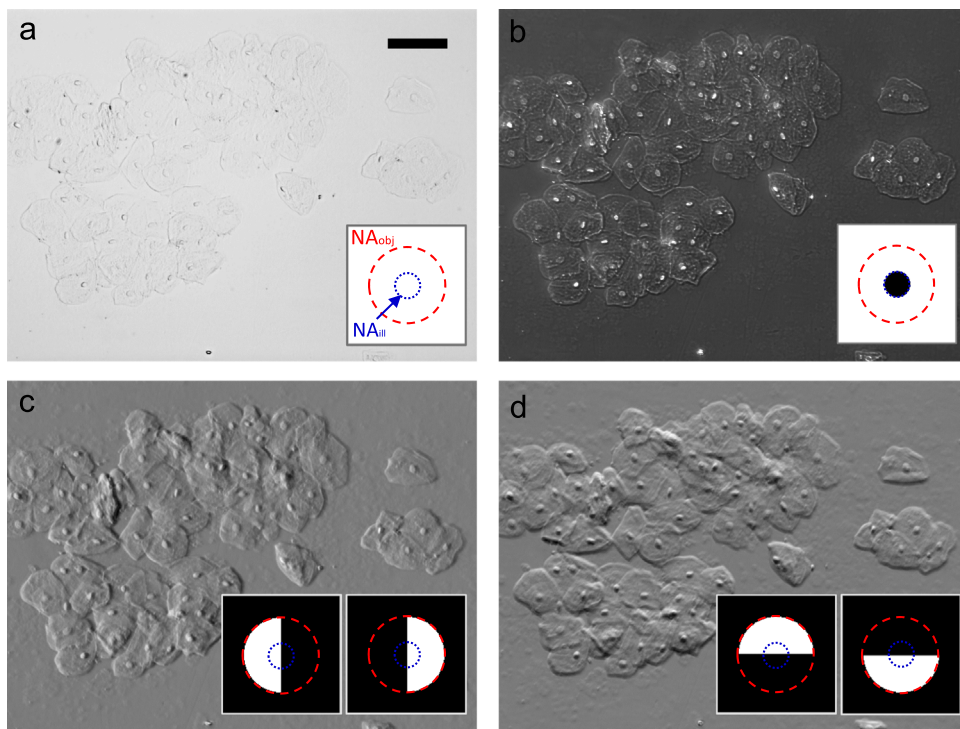


Fig. 2. Contrast-enhancement imaging of unstained cheek cells. (a) Bright field. (b) Dark field. (c) Left-right DPC. (d) Top-bottom DPC. The insets show the corresponding binary patterns displayed on the LCD. Scale bar 100 μm .

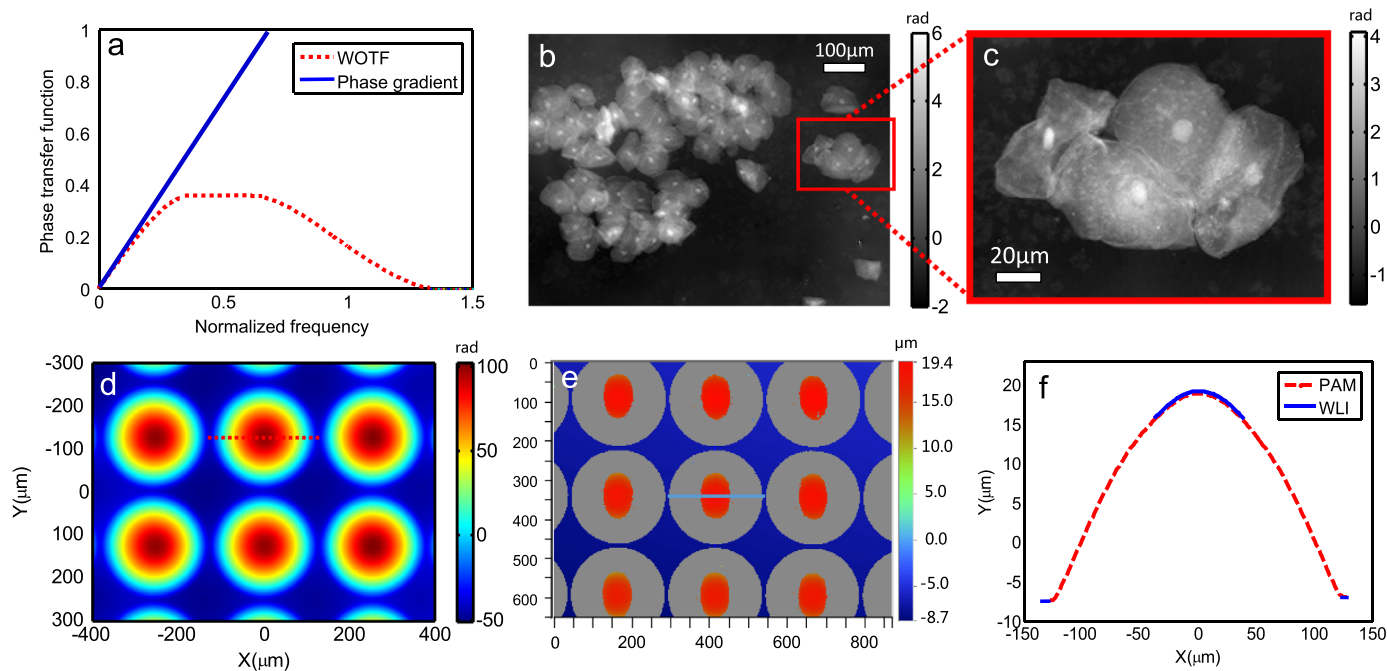


Fig. 3. Quantitative phase imaging and surface profiling. (a) Phase transfer functions based on the WOTF model and ideal phase gradient model ($NA_{obj}=0.3$, $NA_{ill}=0.1$), the frequency coordinate is normalized by NA_{obj}/λ . (b) Quantitative phase map of cheek cells. (c) Quantitative phase map of a small region [corresponding to the red-boxed region in (b)] using a 40X objective ($NA_{obj}=0.6$, $NA_{ill}=0.2$). (d) Phase map of a plano-convex microlens array. (e) Height map measured by WLI. (f) Lens thickness cross-sections corresponding to the line profiles indicated in (d) and (e), respectively. (For interpretation of the references to color in this figure caption, the reader is referred to the web version of this paper.)

shown in Fig. 2(d). Images produced by DPC have a distinctive shadow-cast appearance, rendering the morphology of the otherwise transparent sample into a high-contrast pseudo-relief.

Based on simple geometrical considerations, it follows that these DPC images are directly proportional to the phase gradient in the x or

y direction [20–22]:

$$\nabla\phi \approx \frac{2\pi}{\lambda} \left(\frac{\pi N A_{ill} D_x}{2}, \frac{\pi N A_{ill} D_y}{2} \right). \quad (2)$$

Based on the above relation, the quantitative phase distribution can be conveniently reconstructed through numerical integration. The phase integration algorithms can be interpreted as an inverse gradient filtering process in spatial frequency domain with a linear ramp filter transfer function (Fig. 3(a)). However, it should be noted that the relation Eq. (2) only holds if the object phase is slowly varying with respect to the resolution of the imaging system such that $|\nabla\phi| < NA_{ill}$ [21]. For phase with larger gradient (corresponds to higher spatial frequencies), Eq. (2) generally overestimates the phase contrast signal, and acts as a low pass filter in the phase integration, which in turn causes loss of fine details of the phase reconstruction result. To correct this phase blurring, we replace the inverse gradient filter with a more accurate phase transfer function derived based on the weak-object transfer function (WOTF) model [23,19,18], which takes the effect of illumination coherence as well as the limit objective NA into consideration. As compared in Eq. (2), the two phase transfer functions show good agreement within the lower NA regions, but start to deviate at higher spatial frequencies. The effect of illumination and objective NA can be clearly identified in the more physically correct WOTF based transfer function: it demonstrates a rapid fall after $NA_{obj} - NA_{ill}$, with the cutoff frequency occurs at $NA_{obj} + NA_{ill}$, which coincides with the resolution limit of a partially coherent imaging system. Fig. 3(b) shows the quantitative phase distribution recovered from the two DPC images (Fig. 2(c) and (d)). Besides, a small portion of the whole field of view was imaged with a higher magnification objective (LUCPLFLN40X, $NA_{obj}=0.6$, $NA_{ill}=0.2$) and the corresponding quantitative phase image is shown in Fig. 3(c). These phase images clearly highlight the optically thick nucleus, mitochondria in the cytoplasm, and wrinkled cell membrane of with high resolution and high contrast.

To further verify the quantitiveness of the phase reconstruction, we measured a well-characterized plano-convex microlens array (SUSS, pitch 250 μm , fused silica, refractive index 1.46 at 550 nm). To assess the accuracy of the phase measurement, the same specimen was measured using a white-light interferometer (WLI, Veeco NT9000), as shown in Fig. 3(e). Note the WLI can only provide an incomplete lens profile with the phase

information unrecoverable at the larger phase gradient area due to the very high fringe density. Thickness profiles for a single lens from the array taken along the red-dashed line in Fig. 3(d) and the blue solid line in Fig. 3(e) are compared quantitatively in Fig. 3(f). The height of the microlens was measured to be 25.76 μm with the PAM, which is in reasonable agreement with the WLI result of 26.22 μm , demonstrating its quantitative phase retrieval capability. The fitted radius of curvature (ROC) of our line profile is 286.6 μm , which slightly underestimated the ROC value compared with the manufacturer specifications (297 $\mu\text{m} \pm 5\%$). This small discrepancy can be attributed to the inaccurate determination of the NA_{ill} or the optical imperfection present in the 4f imaging system.

3.3. Multi-perspective imaging

Another important functionality achieved by our PAM is to create images of a thick 3D object from arbitrary perspectives. Conventional microscopes are intrinsically limited to orthographic view, which is always a 2D projection of the 3D scene along the optical axis direction. However, in our PAM, we can modify the shape the aperture so that only the light rays arriving in a small specified region within the whole objective aperture can pass through the LCD. By changing the position of the sub-aperture, different perspective views of the specimen can be obtained and no post-processing is required. To demonstrate the multi-perspective imaging ability of our PAM, two thick samples (honey bee third pair of legs and fern prothallium with young sporophyte) were imaged and their different perspective views are shown in Fig. 4. Note that during this experiment, the microscope condenser diaphragm is full opened in order to achieve the largest possible range for the view shifting (about $\pm 17^\circ$, determined by NA_{obj}). In oblique views, the objects distributed above or below focus laterally shifts in opposite directions, thus enhancing the depth perceptions. Furthermore, the LCD can be dynamically refreshed at a video rate controlled by our computer program, which offers conventional microscopes additional degree-of-freedom to manipulate the virtual viewpoint of the object in an interactive manner (the corresponding AVI format

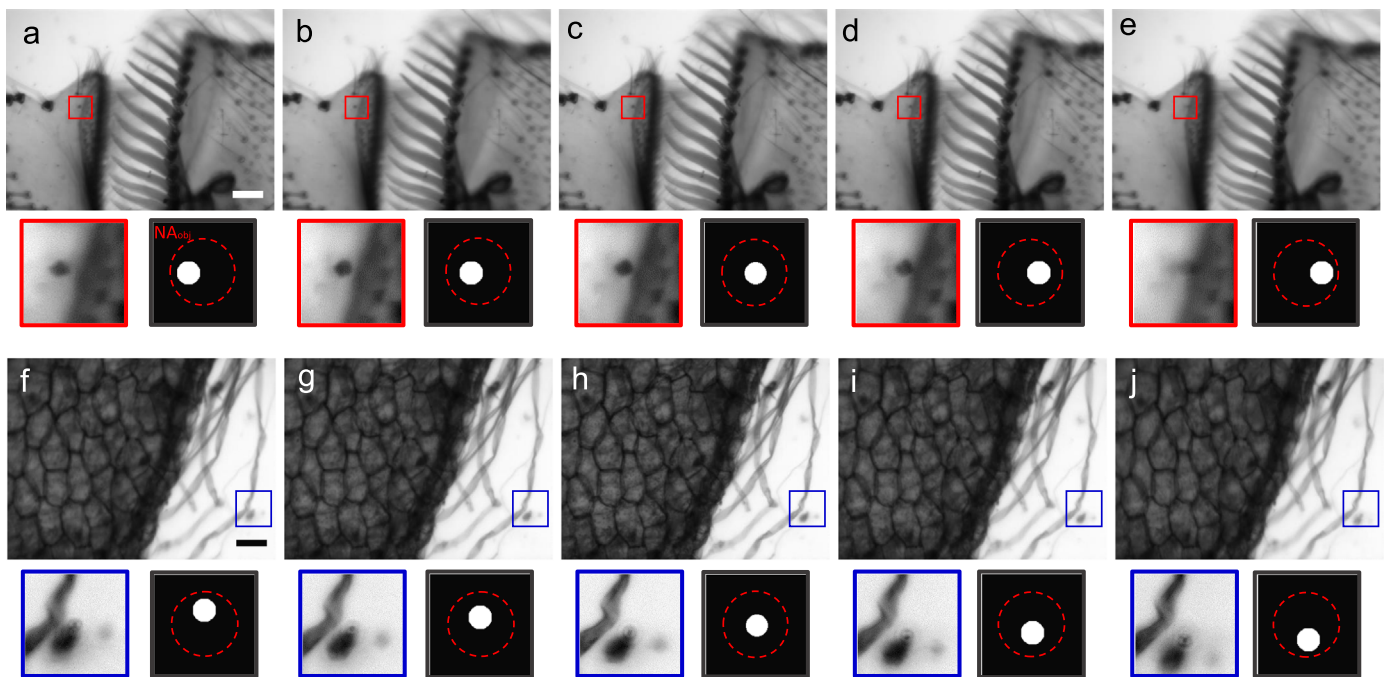


Fig. 4. Multi-perspective imaging of thick samples with corresponding patterns displayed on the LCD. (a)–(e) Honey bee third pair of legs (Media 2). (f)–(j) Fern prothallium with young sporophyte (Media 3). The red/blue-boxed insets show corresponding regions of interest. Scale bars 100 μm . (For interpretation of the references to color in this figure caption, the reader is referred to the web version of this paper.)

movie clips Media 2 and Media 3 are provided). The final captured images has the full pixel number as the camera without sacrificing spatial resolution, and the effective numerical aperture for each view is fully determined by the size of the sub-aperture displayed on the LCD.

3.4. Full resolution light field imaging

Lastly, the reported PAM can also be used for full resolution light field imaging. More specifically, based on geometric optics considerations, one image captured with a small sub-aperture displayed on the LCD just corresponds to a subset of the light field. By capturing images with a small sub-aperture shape scanning through the whole objective pupil, a complete light field can be reconstructed. However, to acquire a light field with a decent angular resolution, for example, 10 by 10 light field views, the size for each sub-aperture is so small that the light collection efficiency of this straightforward acquisition becomes a challenging issue. To solve this problem, we adopt an optimal multiplexing scheme [24] by opening multiple sub-apertures simultaneously at each exposure, and then de-multiplexing individual light field view afterwards. Compared with the sequential scanning, the multiplexed light field acquisition scheme improves the light-gathering efficiency and thus reduces the camera exposure time significantly. By evaluating the noise characteristics and the true signal value, we chose to open 40 out of the whole 10×10 sub-apertures at each exposure. The optimal multiplexing pattern is obtained by solving the corresponding constraint optimization problem based on the projected gradient method [25]. Fig. 5(a) shows 4 different

patterns (out of 100) and their corresponding images of a butterfly mouthpart captured with multiplexing. The demultiplexed 10 by 10 light field cubes are shown in Fig. 5(b). In this experiment, the camera exposure time was set to 63ms, corresponding to a 15 Hz frame rate. By properly synchronizing the LCD and the camera, capturing all 100 multiplexed images only takes less than 7 s. With the complete 4D light field dataset, we can render images with post-capture control of focus. The numerical refocused z-stack is animated in a AVI format movie clip Media 4, and 4 images focused at different depths are shown in Fig. 5(c)–(f), which are obtained by first shearing and then summing the 4D light field [8,12,13]. The synthesized images shows a good agreement with the raw images captured by physically moving the sample stage through focus (Fig. 5(g)–(i), corresponding AVI movie clip Media 5) in terms of both spatial resolution and the signal-to-noise ratio, suggesting that our PAM can accurately acquire the complete 4D light field and render post-exposure refocused images in a physically correct way.

3.5. Imaging of fluorescent specimens

Since the programmable LCD is located at the detection path of the microscope, our PAM can also be applied to fluorescent or self-luminous specimens. This is a major advantage over the programmable illumination schemes based on the LED array or LCD panel arranged at the illumination path of the microscope. In this section, we demonstrate the use of our PAM system for multi-modal fluorescence imaging. The sample is a RFP-labeled dicot

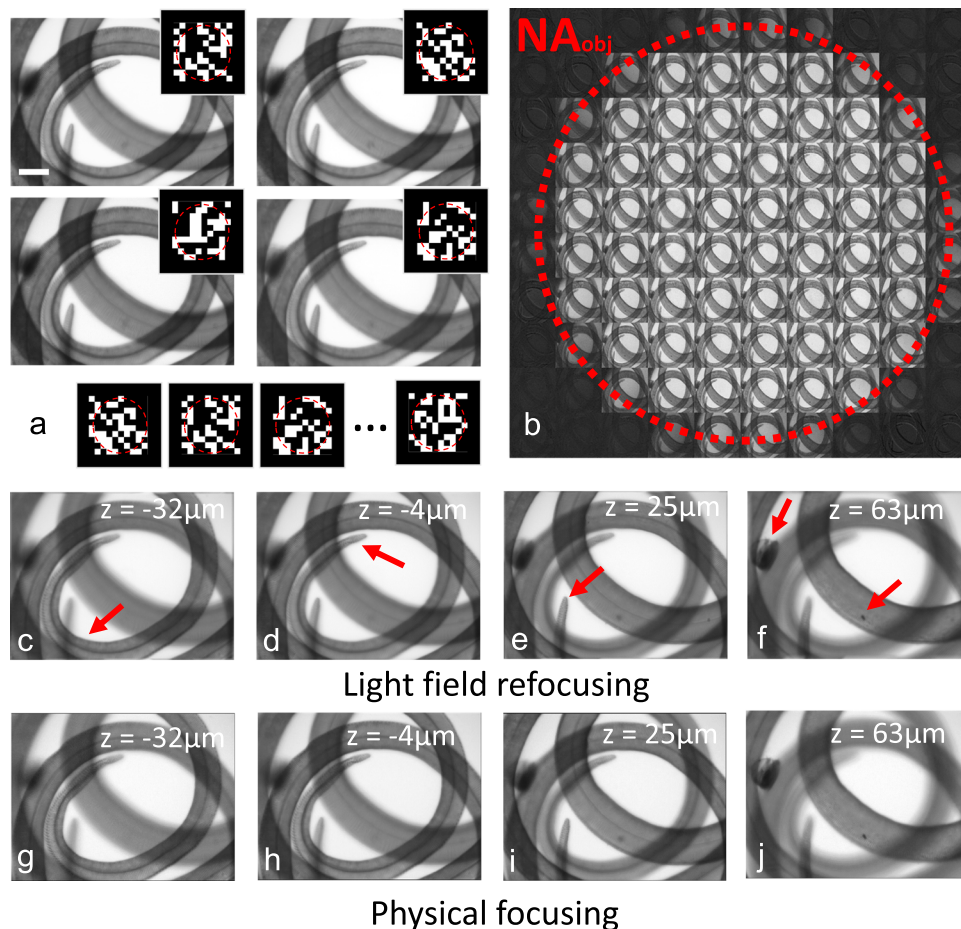


Fig. 5. Full resolution light field imaging of a butterfly mouthpart. (a) Multiplexed light field images with corresponding binary patterns displayed on the LCD. (b) Demultiplexed 10 by 10 light field cubes. (c)–(f) Light field refocused images at different depths (Media 4). (g)–(j) Physical focused images at same depth as (c)–(f) (Media 5). Scale bar 100 μm .

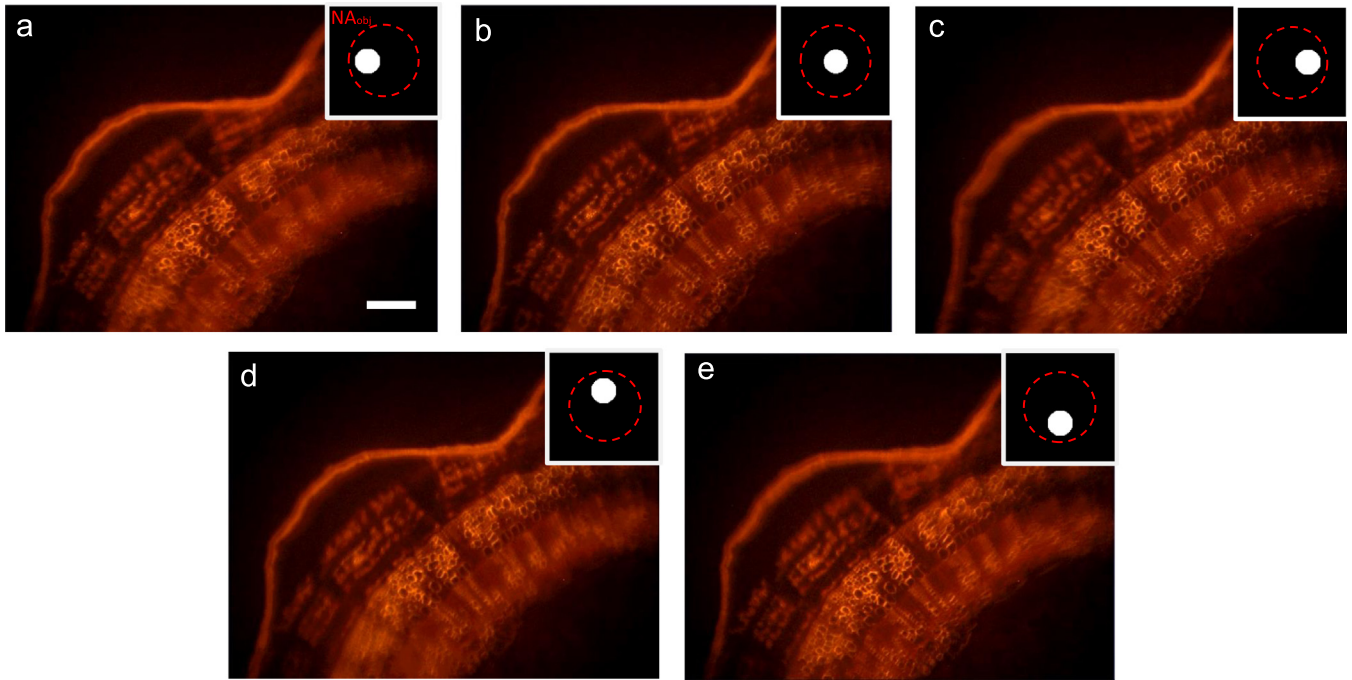


Fig. 6. Multi-perspective imaging of a RFP-labeled dicot stem cross-section (Media 6). The insets show the corresponding binary patterns displayed on the LCD. Scale bar 100 μm .

stem cross-section taken with an Olympus U-FGNA filter (excitation filter: 540–550 nm, dichromatic filter: 570 nm, emission filter: 575–625 nm). We use a 10X 0.3 NA objective lens (UPLFLN10X, Olympus) for both epi-fluorescence illumination and detection and a CCD camera (Olympus UC50) for image acquisition. For fluorescent specimens, only the multi-perspective imaging and the light field imaging modes can be used. In Fig. 6, we show different perspective views of the fluorescent specimen. These images are obtained by laterally shifting the sub-aperture displayed on the LCD. The associated AVI format movie clip is presented in Media 6. Again, the animation illustrates apparent perspective effects. This imaging mode is particularly suited for fluorescent sample since different views can be delivered in single shot and real-time, thus minimizing sample exposure time. Furthermore, increasing the size of sub-aperture displayed on the LCD allows more light to be gathered by the camera, but meanwhile reducing the depth of field.

The same sample was also used to demonstrate the full resolution light field fluorescence imaging. Using the programmable aperture, we can easily capture the full light field with both high spatial resolution and angular resolution by using the light-field multiplexing scheme, as we discussed in Section 3.4. It should be noted that in fluorescence microscopy, of biological sample in particular, the signal levels are typically low due to the limited amount of light obtainable from the small fluorophore. If each light-field image is captured directly (without multiplexing) by sequentially scanning a small pinhole aperture displayed on the LCD, the resultant light field will be quite noisy due to the low signal level. This issue can be significantly alleviated by using the light-field multiplexing. Fig. 7(a) shows the demultiplexed 10 by 10 light field cubes, which is obtained by opening 27 out of the whole 10×10 sub-apertures at each exposure. A comparison of one light field view obtained by direct scanning measurement and multiplexing is clearly illustrated in Fig. 7(b). In both situations, the images are taken with the same exposure time (500 ms). The boost of the signal-to-noise ratio is evident. The advantageous effect of multiplexing can be easily understood if the image noise is purely additive and signal-independent. In such case, the well-

known Hadamard multiplexing yields best SNR improvement over scanning measurement [26]. However, further increasing the number of multiplexed light field views (for example, using the Hadamard code) does not necessarily improve imaging performance, and may even result in detrimental effects on SNR, as shown in Fig. 7(b). This is because of the presence of signal-dependant photon noise (also called Poisson noise since it follows Poisson statistics). The photon noise degrades the performance of multiplexing because of the increase of photo noise by the superposition of multiple signals [25,27]. Therefore, for a practical imaging system where both photon and additive noise present, the number of multiplexed light field views N should be carefully chosen to achieve an optimal trade-off between the two kinds of noise components. The optimal multiplexing number N is found to be 27 in our fluorescence imaging configuration by assessing the camera response and noise level. More details about the noise calibration and the multiplexing code construction can be found in Ref. [25]. With the demultiplexed 10×10 light fields, we can focus the sample at different depths by shearing the light field before summing, as shown in the Fig. 7(c)–(e) and animated in Media 7. Different features at different depths can be clearly distinguished by light field refocusing. This flexibility of post-shot refocusing significantly extends the depth-of-field (DOF) compared to a conventional microscope with fixed aperture.

4. Conclusions

In conclusion, we have demonstrated the feasibility of transforming a standard wide-field microscope into a multi-modal computational microscope by utilizing a LCD as a low-cost transmissive spatial light modulator located at the back aperture of a microscope objective. Different imaging modalities, such as bright field, dark field, differential phase contrast, quantitative phase imaging, multi-perspective imaging, and full resolution light field imaging can be easily achieved by simply creating different binary patterns displayed on the LCD. The LCD is dynamically controlled under the computer software so that different imaging modalities

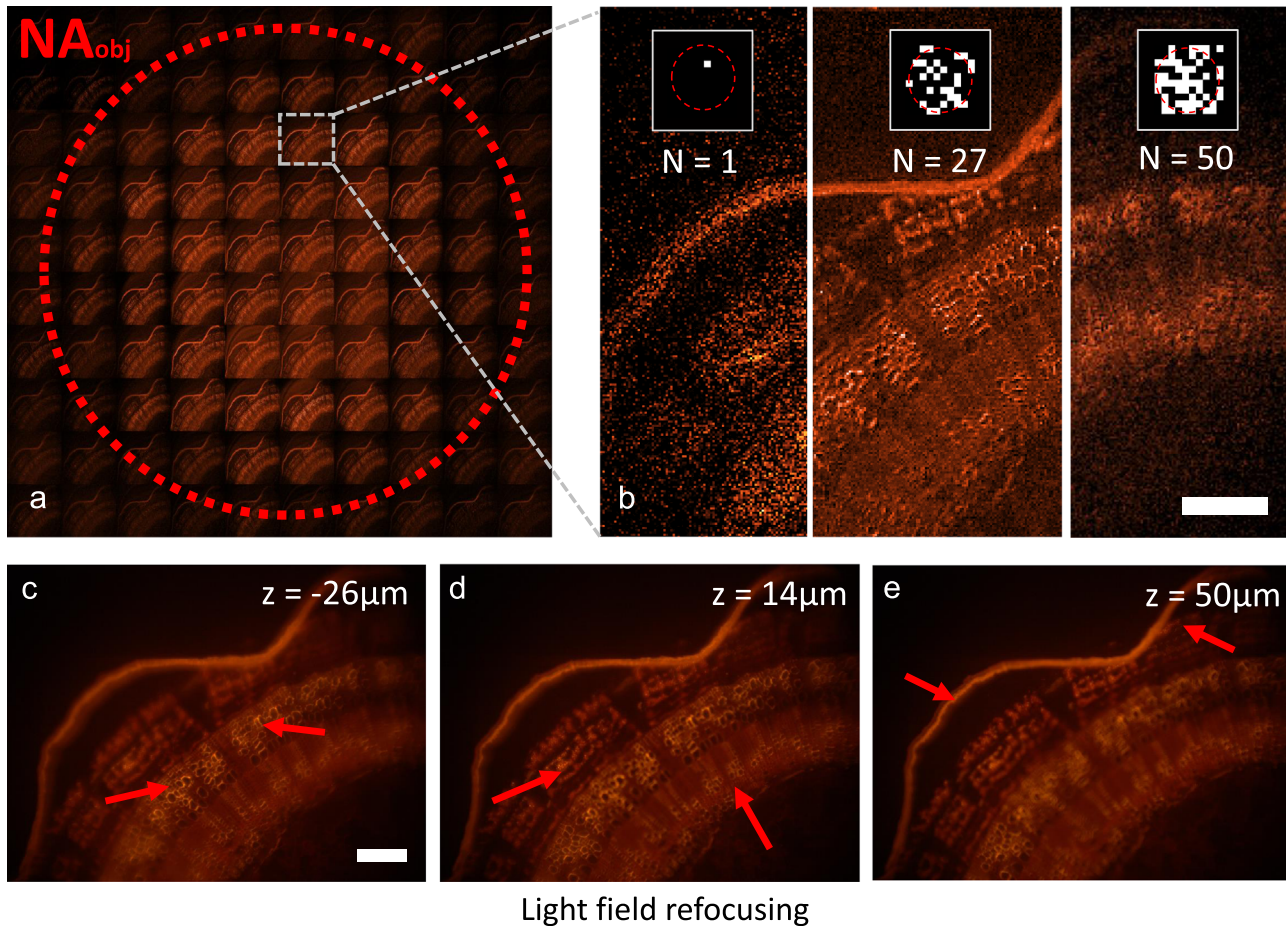


Fig. 7. Full resolution light field imaging of a RFP-labeled dicot stem cross-section. (a) Demultiplexed 10 by 10 light field cubes (multiplexing number $N=27$). (b) Comparison of one light field view obtained by direct scanning measurement, light-field multiplexing scheme $N=27$, and $N=50$. (c-e) Light field refocused images at different depths (Media 7). Scale bar $100\mu m$.

can be realized and switched with a single keystroke, with no moving parts. In addition, our PAM is fully backward compatible with most standard bright field or fluorescence microscopes. The versatility and effectiveness of the PAM has been demonstrated by imaging of various types of specimens, including unstained cheek cells, microlens array, butterfly mouthpart, and RFP-labeled dicot stem cross-section.

The recent emergence of modern optical devices such as high resolution spatial light modulator (SLM) or digital mirror device (DMD) has enabled a multitude of research activities over the past decade to reinvent microscopic imaging in unconventional ways [4,10,11]. As the key component employed in our PAM system, the LCD panel is acted as a transmissive SLM implemented at the back aperture of a microscope objective. The LCD selectively let the light from some region of the aperture to pass through, while other light are blocked. The reason why we choose to use a low cost, low resolution LCD instead of a high resolution SLM or DMD is four-fold. First, the LCD used in our system is only a optical switch for light field, therefore it only need to realize binary amplitude modulation. While most of high resolution liquid crystal SLM commercially available can only manipulate the phase of the light incident on them. Second, the spatial resolution of the LCD only relates to the number of resolvable light field views and does not affect the spatial resolution of the final reconstructed image. Since humans are more tolerant of low angular resolution than low spatial resolution, a 10×10 light field reconstruction is sufficient to produce artifact-free refocused images, as demonstrated in our experiments. On the other hand, fundamental physical limits of

image acquisition as well as the uncertainty principle in optics also suggests that the light field is only measurable when the size of sub-aperture is large enough for a meaningful detection [28]. Third, the high resolution SLM or DMD tend to act like a grating, which usually creates numerous undesired diffraction orders. Using a low resolution LCD can help alleviate such problem. Lastly, the cost of the low resolution LCD used here is much lower (only ~ 20 USD) than the high resolution SLM and DMD.

Finally, it should be mentioned that one limitation of the PAM system lies in the light leakage of the each pixel on the ‘off-state’ (each pixel does not become completely opaque when turned ‘off’). The contrast ratio (“white” transmittance divided by the “black” transmittance) of the LCD employed in our system is measured to be 82:1 with use of a simple “full on/full off” method. The light leakage leads to a residual background on each captured image. The residual background can be digitally removed from the measurements by background subtraction (with a additional “full off” image). Moreover, the light-field multiplexing scheme also helps mitigate such problem. In the further, we would like to optimize the multiplexing scheme by accounting for the light leakage of LCD, and further explore the great potential of the PAM for fluorescence imaging applications.

Acknowledgments

This work was supported by the National Natural Science Fund of China (11574152, 61505081), Six Talent Peaks project (2015-

DZXX-009, Jiangsu Province, China) and '333 Engineering' research project (BRA2015294, Jiangsu Province, China), Fundamental Research Funds for the Central Universities (30915011318), and Open Research Fund of Jiangsu Key Laboratory of Spectral Imaging & Intelligent Sense (3092014012200417). C. Zuo thanks the support of the 'Zijin Star' program of Nanjing University of Science and Technology.

Appendix A. Supplementary data

Supplementary data associated with this paper can be found in the online version at <http://dx.doi.org/10.1016/j.optlaseng.2015.12.012>.

References

- [1] Mann C, Yu L, Lo C-M, Kim M. High-resolution quantitative phase-contrast microscopy by digital holography. *Opt Express* 2005;13:8693–8.
- [2] Wang Z, Millet L, Mir M, Ding H, Unarunotai S, Rogers J, et al. Spatial light interference microscopy (slim). *Opt Express* 2011;19:1016–26.
- [3] Zuo C, Chen Q, Qu W, Asundi A. Noninterferometric single-shot quantitative phase microscopy. *Opt Lett* 2013;38:3538–41.
- [4] Rodrigo JA, Alieva T. Illumination coherence engineering and quantitative phase imaging. *Opt Lett* 2014;39:5634–7.
- [5] Gustafsson MGL. Surpassing the lateral resolution limit by a factor of two using structured illumination microscopy. *J Microsc* 2000;198:82–7.
- [6] Gao P, Pedrini G, Osten W. Structured illumination for resolution enhancement and autofocusing in digital holographic microscopy. *Opt Lett* 2013;38:1328–30.
- [7] Zheng G, Horstmeyer R, Yang C. Wide-field, high-resolution Fourier ptychographic microscopy. *Nat Photon* 2013;7:739–45.
- [8] Levoy M, Ng R, Adams A, Footer M, Horowitz M. Light field microscopy. *ACM Trans Graph* 2006;25:924–34.
- [9] Prevedel R, Yoon Y-G, Hoffmann M, Pak N, Wetzstein G, Kato S, et al. Simultaneous whole-animal 3d imaging of neuronal activity using light-field microscopy. *Nat Methods* 2014;11:727–30.
- [10] Samson EC, Blanca CM. Dynamic contrast enhancement in widefield microscopy using projector-generated illumination patterns. *New J Phys* 2007;9:363.
- [11] Maurer C, Jesacher A, Bernet S, Ritsch-Marte M. What spatial light modulators can do for optical microscopy. *Laser Photon Rev* 2011;5:81–101.
- [12] Zheng G, Kolner C, Yang C. Microscopy refocusing and dark-field imaging by using a simple led array. *Opt Lett* 2011;36:3987–9.
- [13] Tian L, Wang J, Waller L. 3d differential phase-contrast microscopy with computational illumination using an led array. *Opt Lett* 2014;39:1326–9.
- [14] Liu Z, Tian L, Liu S, Waller L. Real-time brightfield, darkfield, and phase contrast imaging in a light-emitting diode array microscope. *J Biomed Opt* 2014;19:106002.
- [15] Guo K, Bian Z, Dong S, Nanda P, Wang YM, Zheng G. Microscopy illumination engineering using a low-cost liquid crystal display. *Biomed Opt Express* 2015;6:574–9.
- [16] Zuo C, Sun J, Feng S, Hu Y, Chen Q. Programmable colored illumination microscopy (pcim): a practical and flexible optical staining approach for microscopic contrast enhancement. *Opt Lasers Eng* 2016;78:35–47.
- [17] Zuo C, Chen Q, Tian L, Waller L, Asundi A. Transport of intensity phase retrieval and computational imaging for partially coherent fields: the phase space perspective. *Opt Lasers Eng* 2015;71:20–32.
- [18] Hamilton DK, Sheppard CJR. Differential phase contrast in scanning optical microscopy. *J Microsc* 1984;133:27–39.
- [19] Mehta SB, Sheppard CJR. Quantitative phase-gradient imaging at high resolution with asymmetric illumination-based differential phase contrast. *Opt Lett* 2009;34:1924–6.
- [20] Chamot SR, Dainty C, Esposito S. Adaptive optics for ophthalmic applications using a pyramid wavefront sensor. *Opt Express* 2006;14:518–26.
- [21] Burvall A, Daly E, Chamot SR, Dainty C. Linearity of the pyramid wavefront sensor. *Opt Express* 2006;14:11925–34.
- [22] Parthasarathy AB, Chu KK, Ford TN, Mertz J. Quantitative phase imaging using a partitioned detection aperture. *Opt Lett* 2012;37:4062–4.
- [23] Streibl N. Three-dimensional imaging by a microscope. *J Opt Soc Am A* 1985;2:121–7.
- [24] Liang C-K, Lin T-H, Wong B-Y, Liu C, Chen HH. Programmable aperture photography: multiplexed light field acquisition. *ACM Trans Graph* 2008;27:55:1–10.
- [25] Ratner N, Schechner Y. Illumination multiplexing within fundamental limits. In: 2007 IEEE Conference on computer vision and pattern recognition, CVPR '07; 2007. p. 1–8.
- [26] Sloane NJA, Harwit M. Masks for Hadamard transform optics, and weighing designs. *Appl Opt* 1976;15:107–14.
- [27] Streeeter L, Burling-Claridge GR, Cree MJ, Künnemeyer R. Optical full Hadamard matrix multiplexing and noise effects. *Appl Opt* 2009;48:2078–85.
- [28] Zhang Z, Levoy M. Wigner distributions and how they relate to the light field. In: 2009 IEEE International Conference on Computational Photography (ICCP); 2009. p. 1–10.